Volume 6
Number 9
7 May 2025
Pages 2705–3004

Materials Advances

rsc.li/materials-advances

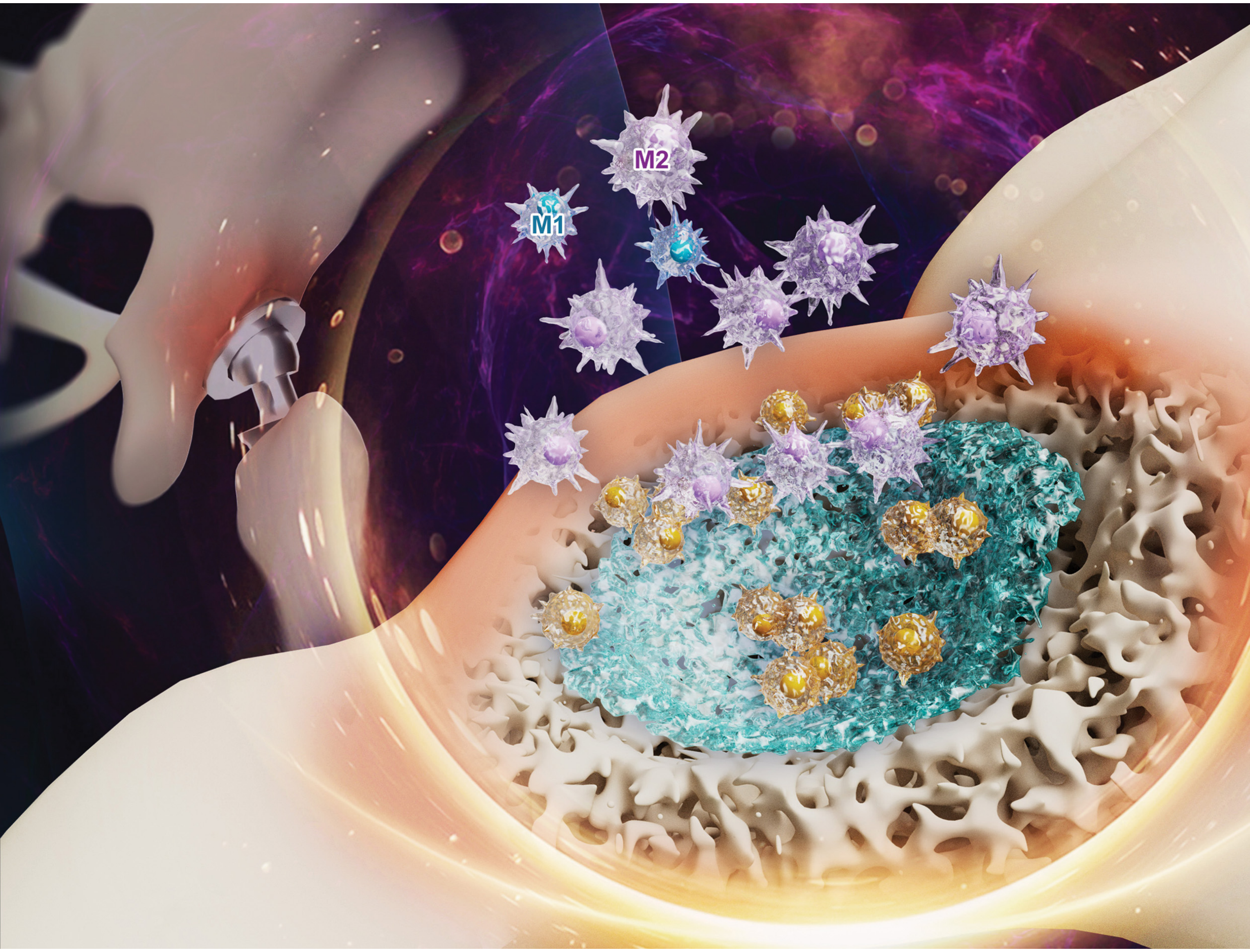

ISSN 2633-5409

ROYAL SOCIETY OF CHEMISTRY

PAPER
Xianlong Zhang, Chunming Lyu *et al.*
DFO-modified polydopamine sulfonated PEEK enhances osseointegration through macrophage immunomodulation and osteogenic differentiation of BMSCs

Materials Advances

ROYAL SOCIETY OF CHEMISTRY

PAPER

View Article Online
View Journal | View Issue

Check for updates

Cite this: *Mater. Adv.*, 2025, **6**, 2781

DFO-modified polydopamine sulfonated PEEK enhances osseointegration through macrophage immunomodulation and osteogenic differentiation of BMSCs†

Shengjie Wang,‡[a] Wei Liu,‡[a] Chao Yang,[a] Xianlong Zhang*[a] and Chunming Lyu *[bc]

Received 29th November 2024,
Accepted 27th March 2025

DOI: 10.1039/d4ma01179a

rsc.li/materials-advances

This study aimed to develop a novel artificial joint prosthesis material with osteogenic properties. Deferoxamine mesylate (DFO) was immobilized on the porous surface of sulfonated polyetheretherketone (SPEEK) using polydopamine (PDA), resulting in a novel material designated as DFO-PDA@SPEEK (DFO-PS). DFO-PS induced macrophage M2 phenotype polarization, reduced inflammatory factor expression, promoted osteogenic differentiation of bone marrow mesenchymal stem cells (BMSCs), and enhanced implant osseointegration and osteogenic capacity. *In vitro* evaluation demonstrated that DFO-PS significantly modulated immune and inflammatory responses, promoted angiogenesis, and enhanced osteogenic differentiation. In the rat model with femoral bone defects, in comparison to the control group, the DFO-PS group exhibited a 1.22-fold increase in trabecular thickness and a 1.51-fold enhancement in maximum pull-out force. This work demonstrates that DFO-PS is a promising material for constructing multifunctional implants with biomineralization and immunomodulation properties for bone joint replacement.

1. Introduction

Joint replacement surgery is the most crucial intervention for end-stage bone and joint disorders, including osteoarthritis, deformities, and femoral head necrosis.[1,2] However, approximately 18% of patients experience aseptic loosening postoperatively, imposing substantial economic burdens on both society and patients, highlighting the urgent need for developing next-generation prosthetic materials that enhance osseointegration between implants and surrounding bone tissue.[3] Polyetheretherketone (PEEK), an aromatic polymer compound containing chain segments in its molecular backbone, has emerged as one of the most promising polymeric implant materials in orthopedics due to its excellent biocompatibility, the absence of imaging artifacts, its bone-like elastic modulus, and its superior wear resistance.[4,5] Nevertheless, the long-term *in vivo* application of PEEK implants is limited by its poor osseointegration and weak anti-infection capabilities due to surface bioinertness.[6,7] Polydopamine (PDA) exhibits multiple advantageous properties, including hydrophilicity, appropriate roughness, biocompatibility, antibacterial activity, cell adhesion, and osteogenic potential. These characteristics make it suitable for modifying orthopedic implant surfaces, promoting bone reconstruction through its strong adhesive properties and dopamine (DA) release.[8] The high adhesive properties of PDA enable it to serve as an intermediate layer facilitating "dual modification" with other functional bone reconstruction materials, such as growth factors, nanoparticles, peptides, and hydrogels.[9] During bone remodeling, PDA degradation leads to the release of DA into the surrounding microenvironment, playing a crucial role in regulating DA receptors on osteoblasts and osteoclasts.[10]

Deferoxamine mesylate (DFO), a hexadentate molecule that binds to plasma iron in a 1 : 1 molar ratio and forms aluminoxanes with plasma aluminum, is a chelating agent used to treat iron and aluminum toxicity and is eliminated through biliary or renal excretion.[11] It was reported that DFO reduces the release of local inflammatory factors (TNF-α, IL-1β, and IL-6) and fibrosis following radiation or surgery while increasing local

---

[a] Department of Orthopaedic Surgery, Shanghai Sixth People's Hospital Affiliated to Shanghai Jiao Tong University School of Medicine, 600 Yishan Road, Shanghai 200233, China. E-mail: dr_zhangxianlong@sjtu.edu.cn; Fax: +86 021-24058101; Tel: +86 021-24058101

[b] Experiment Center for Science and Technology, Shanghai University of Traditional Chinese Medicine, Shanghai 201203, China. E-mail: chunming83g@126.com; Tel: +86 021-51323044

[c] Qinghai Province Key Laboratory of Tibetan Medicine Pharmacology and Safety Evaluation, Northwest Institute of Plateau Biology, Chinese Academy of Sciences, Xining 810008, China

† Electronic supplementary information (ESI) available. See DOI: https://doi.org/10.1039/d4ma01179a

‡ These authors contributed equally to this work.

vascular endothelial growth factor (VEGF) expression.[12] Momeni *et al.*[13] documented the clinical application of DFO in a young male patient undergoing maxillary distraction osteogenesis, observing greater new bone area and density in the DFO treatment group. Lintel *et al.*[14] found that DFO promotes local collagen deposition and microvessel growth, improving radiation therapy-induced wound healing in mice. It was also reported that DFO, in conjunction with three-dimensional scaffolds, enhances human BMSC osteogenic gene expression and vascularization at fracture sites.[15]

Based on these previous research studies, a scientific hypothesis is proposed in this study: DFO loaded PDA-SPEEK may achieve dual advantages. First, PDA's adhesive properties serving as an intermediate layer could facilitate the attachment of functional bone reconstruction materials (such as DFO), thereby enhancing the osseointegration of SPEEK implants. Second, exogenously released DFO could promote macrophage M2 polarization, protecting bone formation from inflammatory inhibition in the implant microenvironment while enhancing osteogenic differentiation of BMSCs. Consequently, functional bone reconstruction materials may achieve better contact and fusion with bone tissue following artificial joint implantation, improving the stability and durability of prosthetic-bone connections.

2. Materials and methods

The animal experiments were conducted at the Shanghai Laboratory Animal Center, Chinese Academy of Sciences, under the approval of the Animal Care and Experimentation Committee (approval number: 20211201039).

2.1. Preparation, characterization, and biocompatibility of DFO-PS

2.1.1. Preparation of DFO-PS. SPEEK (sulfonated polyetheretherketone) was synthesized following the method described by Liu *et al.*[16] PEEK (Ensinger Company, Nufringen, Germany, 10074862684875) was cut into rod-shaped specimens (2 mm diameter × 10 mm length) or disc-shaped specimens (10 mm diameter × 1 mm thickness). The PEEK samples were sulfonated with 98% concentrated sulfuric acid at room temperature for 8 min, rinsed thrice with deionized water, and then treated in a hydrothermal vessel at 120 °C for 4 h to remove residual acidic substances, resulting in a three-dimensional porous SPEEK material. The specimens were divided into five groups, with 1 mL reagent added to each beaker. The control group contained pure SPEEK without dopamine powder. The other 4 groups received 0.01 M Tris buffer (pH 8.5) and 3 mg mL^{-1} dopamine powder (A303863, Shanghai Aladdin Biochemical Technology Co., Ltd, Shanghai, China). Then, DFO mesylate (D873692, Macklin Bio-Chem Technology, Shanghai, China) solution was added, and the concentration in the four beakers was 0, 1, 5, and 25 mg mL^{-1}, respectively. The mixtures were agitated at 5 rpm for 1 h (SK-R1807-E, SHKTYQ, Beijing, China) and dried at room temperature for 1 h. Subsequently, 5 sets of materials were prepared (Con standing for the SPEEK group, PS standing for the PDA@SPEEK group, 1DFO-PS standing for the 1 mg mL^{-1} DFO-PDA@SPEEK group, 5DFO-PS standing for the 5 mg mL^{-1} DFO-PDA@SPEEK group, and 25DFO-PS standing for the 25 mg mL^{-1} DFO-PDA@SPEEK group).

2.1.2. Material parameter analysis of DFO-PS. Contact angles were measured using an LSA MOB-L contact angle meter (LAUDA Scientific; Hazi, Germany). Drug release profiles in phosphate-buffered saline (PBS) were determined using a UV spectrophotometer at 340 nm wavelength (752N, Shanghai Jingke, Shanghai, China). Surface morphology and structural characteristics were examined using an FEI NovaNano450 scanning electron microscope (JEOL, JSM-631LV, Tokyo, Japan).

2.1.3. Cellular biocompatibility of DFO-PS. RAW264.7 cells (BS-C00567843, Shanghai Binsui Biotechnology Co. LTD) and rBMSCs (STCC5011, Wuhan Zishan Biotechnology Co. Ltd) were cultured in DMEM supplemented with 10% fetal bovine serum (SH3010902HI, Gibco, Grand Island, USA). Biocompatibility was assessed through cell immunofluorescence (LSM 510 meta, Zeiss, Oberkochen, Germany) and scanning electron microscopy (JEOL, JSM-6310LV, Tokyo, Japan), examining cytoskeleton, morphology, adhesion, and pseudopodia formation. Cell proliferation was evaluated using the CCK-8 assay (C0038, Beyotime Bio-Tech, Shanghai, China), and lactate dehydrogenase (LDH) levels were measured using ELISA (C0017, Beyotime Bio-Tech, Shanghai, China).

2.1.4. Biocompatibility of DFO-PS *in vivo*. 25DFO-PS was subcutaneously implanted in BALB/c mice (Shanghai SLAC Laboratory Animal Co., Ltd, Shanghai, China). The body weight was monitored at various time points. Peripheral blood biochemistry was analyzed using an automatic biochemical analyzer (ADVIA2400, Zeiss, Oberkochen, Germany), and blood cell counts were measured using an automatic hematology analyzer (BC6800, Mindray, Shenzhen, China). Heart, liver, spleen, lung, and kidney tissues were harvested at weeks 1 and 4 for H&E staining and examined under an optical microscope (LSM 510 meta, Zeiss, Oberkochen, Germany).

2.2. Effects of DFO-PS on the M2 polarization of the macrophage

In vitro and *in vivo* experiments were conducted to evaluate the effects of DFO-PS on macrophage M2 polarization and its osteogenic mechanisms.

For *in vitro* studies, five groups of materials (10 mm × 10 mm × 1 mm discs) were placed in 24-well plates (n = 3 per group). RAW264.7 cells (5×10^5 cells per well) were seeded and cultured in DMEM supplemented with 100 U mL^{-1} penicillin, 100 U mL^{-1} streptomycin, and 10% FBS at 37 °C with 5% CO_2. Culture medium was replaced after 24 h of cell attachment. After 3 days of culture (80% confluence), the secretion of IL-4, IL-10, TNF-α, and IL-6 was measured using ELISA. The mRNA expression levels of polarization markers (CD86 and CD163) and osteogenic factors (BMP-2, VEGF) were analyzed by RT-PCR. Immunofluorescence staining was performed to assess iNOS and CD206 (Mannose receptor) protein expression.

For *in vivo* studies, air pouches were created by subcutaneous injection of 5 mL of sterile air into BALB/c mice dorsa.

After 3 days, sterilized material discs from the five groups were implanted into the air pouches under sterile conditions, respectively. Animals were maintained under SPF conditions with free access to water and food. After 1 week, the implant sites were irrigated with 1 mL of PBS, and the lavage fluid was collected for IL-4, IL-10, TNF-α, and IL-6 analysis by ELISA. Surrounding tissues were harvested for RT-PCR analysis of CD86, CD163, BMP-2, and VEGF expression, and immunofluorescence examination of iNOS and CD206.

2.3. DFO-PS enhanced rBMSC osteogenic differentiation *in vitro*

Two sets of *in vitro* experiments were conducted: direct osteogenic differentiation and macrophage polarization-induced osteogenic differentiation.

Material discs (10 mm × 10 mm × 1 mm) from five groups (Con, PS, 1DFO-PS, 5DFO-PS, and 25DFO-PS) were placed in a 24-well plate ($n = 3$ per group). RAW264.7 cells or rBMSCs (5×10^5 cells per well) were cultured in DMEM supplemented with 100 U mL^{-1} penicillin, 100 U mL^{-1} streptomycin, and 10% FBS at 37 °C with 5% CO_2. Conditioned medium (CM) was prepared by mixing the RAW264.7 culture supernatant with complete DMEM (1 : 1).

For the transwell migration assay, rBMSCs (1×10^5 cells per sample) were seeded in the upper chamber of transwells. Two experimental setups were designed to evaluate both direct and indirect effects on rBMSC migration. Direct effects: material discs from different experimental groups were placed in the lower chamber containing DMEM to assess their direct influence on rBMSC migration. Indirect macrophage-mediated effects on cell migration: conditioned medium collected from RAW264.7 cells previously cultured with different material groups was added to the lower chamber, without the presence of material discs, to evaluate the macrophage-mediated effects on rBMSC migration. After 24 hours of incubation, migrated cells on the bottom surface of the transwell membrane were quantified using optical microscopy.

For osteogenic differentiation studies, rBMSCs were cultured with either DMEM or CM for 14 days. Osteogenic gene expression (ALP, OCN, COL-1, BMP-2, OPN, RUNX2, BSP, and OC) was analyzed by RT–PCR. ALP staining and Alizarin Red S (ARS) staining were performed to assess mineralization capacity and calcium deposition, respectively.

2.4. DFO-PS enhanced rBMSC osteogenic differentiation *in vivo*

2.4.1. Animal model establishment. Following the study of Sang *et al.*,[17] the surgical protocol was performed as follows: Rats were anesthetized with 3% pentobarbital sodium *via* intraperitoneal injection. After anesthesia, the right hind limb was shaved and thoroughly sterilized. A 1-cm incision was made at the medial aspect of the right knee. Using an electric drill and a K-wire, a 2-mm diameter hole was created vertically through the intercondylar region of the right femur. Cylindrical implants (2 mm × 2 mm × 10 mm) of different materials (Con, PDA, 1DFO-PS, 5DFO-PS, and 25DFO-PS) were then placed into the femoral intercondylar space, respectively ($n = 3$ per group). The incision was carefully sutured. The rats were maintained under specific-pathogen-free (SPF) conditions with free access to water and food for 8 weeks post-surgery.

2.4.2. Sequential fluorescent labeling and Van Gieson staining. Sequential fluorescent labeling was performed by intraperitoneal injection of Alizarin Red S (30 mg kg^{-1}, AL, Sigma-Aldrich, USA) and Calcein (20 mg kg^{-1}, CA, Sigma-Aldrich, USA) at weeks 3 and 6 post-surgery. At week 8, femurs with implants were harvested, fixed in 10% paraformaldehyde, dehydrated in ethanol, and embedded in methylmethacrylate without decalcification. Sections (50 μm) were prepared using a Leica SP1600 saw microtome (Munich, Germany) and analyzed by confocal laser scanning microscopy (CLSM). Van Gieson's picrofuchsin staining was performed for histological analysis.

2.4.3. Micro-CT analysis. Specimens were scanned using a Micro-CT instrument (Skyscan 1172, Bruker Micro-CT, Munich, Germany) at 18 μm resolution over 360°. Three-dimensional reconstruction was performed using Nrecon software, and the CTAn program analyzed the following parameters within a 0.5 mm radius of the implant: bone-implant contact (BIC, %), bone mineral density (BMD), bone volume fraction (BV/TV, %), trabecular number (Tb.N, mm^{-1}), trabecular thickness (Tb.Th, μm), and trabecular separation (Tb.Sp).

2.4.4. Pull-out testing. At week 8, three samples per group were tested for pull-out strength. Specimens were mounted in steel fixtures using bone cement and tested at a loading rate of 1 mm min^{-1}. Load-displacement curves were recorded, with maximum load defined as the pull-out force.

2.5. Real-time quantitative PCR

Total RNA was isolated from dorsal skin tissues, RAW264.7 cells, or rBMSCs using Trizol (12183555, Invitrogen, California, USA) and reverse transcribed using reverse transcriptase (A48571, Thermo Fisher Scientific Inc., Waltham, USA). RT-PCR was performed in 96-well plates using the SYBR Premix Ex Taq kit (RR001B, TaKaRa, Dalian, China) with 20 μL reaction volume on an ABI 750 system (Applied Biosystems, Carlsbad, USA). PCR conditions were 5 min initial denaturation at 94 °C, followed by 36 cycles at 94 °C for 30 s, annealing for 40 s, and extension at 72 °C for 40 s. The reaction was completed with a final extension at 72 °C for 5 min. Data were normalized to GAPDH and analyzed using the $2^{-\Delta\Delta CT}$ method ($n = 3$). All primer sequences were obtained from Sangon (Shanghai Shengong Biological Engineering Co., LTD Shanghai, China) (Table 1).

2.6. Statistical analysis

Graphpad Prism 9 (Graphpad Software, La Jolla, California) was used to perform the statistical analysis. The data were presented as the mean ± standard deviation (mean ± SD). Unpaired Student's *t* test was used to determine significances between two groups, while multiple groups were compared by one-way ANOVA. Statistical significance was defined as $p < 0.05$ for all analyses.

Table 1 Primers for target genes

Target gene	Oligonucleotide sequence
Mice CD89	5′-TGGGCGCAGAGAAACTTGAT-3′ (forward) 5′-AAGCCCGTGTCCTTGATCTG-3′ (reverse)
Mice CD163	5′-GTGGTCAACTCCGCTTGGTA-3′ (forward) 5′-CTTGGGGCACCATCTGTGAT-3′ (reverse)
Mice BMP-2	5′-AACGAGAAAAGCGTCAAGCC-3′ (forward) 5′-AGGTGCCACGATCCAGTCAT-3′ (reverse)
Mice VEGF	5′-GCAAGAGAAGACACGGTGGT-3′ (forward) 5′-CAGGAGGTGGGGTAAGGAG-3′ (reverse)
Rats BMP-2	5′-AGTAGTTTCCAGCACCGAATTA-3′ (forward) 5′-CACTAACCTGGTGTCCAATAGT-3′ (reverse)
Rats OPN	5′-CTTGAGCATTCCAAAGAGAGC-3′ (forward) 5′-CTTGTGGCTGTGAAACTTGTG-3′ (reverse)
Rats RUNX-2	5′-GCTGTTGTGATGCGTATTCCC-3′ (forward) 5′-TTGAACCTGGCCACTTGGTT-3′ (reverse)
Rats BSP	5′-ACAACACTGCGTATGAAACCTATGAC-3′ (forward) 5′-AGTAATAATCCTGACCCTCGTAGCC-3′ (reverse)
Rats OC	5′-AGGGATGAAGCGTTTCTTAGGTTTTG-3′ (forward) 5′-AGGATGCTGTGGTTGGTGACTG-3′ (reverse)
Rats GAPDH	5′-AGTGCCAGCCTCGTCTCATG-3′ (forward) 5′-GATGGTGATGGGTTTCCCGT-3′ (reverse)

3. Results

3.1. Material characterization of DFO-PS

With increasing DFO concentration, the drug accumulation on the porous surface became denser, leading to faster release rates and higher maximum release concentrations of DFO-PS (Fig. 1B). Due to the poor solubility of DFO, the liquid contact angles of DFO-PS gradually increased with higher DFO concentrations (Fig. 1C). Fig. 1D shows the scanning electron microscopy images of DFO-PS. Through surface modification methods, DFO was successfully loaded onto the surface and within the pores of SPEEK. In summary, DFO was effectively loaded onto both the surface and internal pores of SPEEK, providing a good foundation for the osteogenic modification of SPEEK.

3.2. Biocompatibility analysis of DFO-PS in RAW264.7 macrophages and rBMSCs and in rats

To evaluate the potential cytotoxicity of DFO-PS, RAW264.7 macrophages and rBMSCs were selected as experimental models. LDH release and cell viability assays revealed that DFO concentrations exceeding 64 mg mL^{-1} resulted in elevated LDH release and decreased cell numbers (Fig. 2B). Based on these findings, DFO concentrations of 1, 5, and 25 mg mL^{-1} were selected to modify PS materials, yielding 1DFO-PS, 5DFO-PS, and 25DFO-PS, respectively.

As illustrated in Fig. 2A, both RAW264.7 and rBMSCs exhibited favorable adhesion characteristics on Con (SPEEK), PS (PDA-SPEEK), and 25DFO-PS (25DFO-PDA-SPEEK) surfaces, with extensive pseudopod formation. Additionally, immunofluorescence analysis revealed well-developed and uniformly distributed cytoskeletal structures (Fig. 2C). While high DFO concentrations could lead to cell injury and death, the maximum DFO-PS concentration was established at 25 mg mL^{-1} to ensure biocompatibility.

In vivo biocompatibility was assessed using a murine model. A subcutaneous implantation of 25 mg mL^{-1} DFO-PS showed no significant reduction in body weight over a 4-week observation period (Fig. 2D). Histological examination of major organs using H&E staining at days 0, 7, and 28 revealed no pathological abnormalities across all experimental groups (Fig. 2E). At 4 weeks post-implantation, peripheral blood analysis was conducted to evaluate hematological parameters, including RDW, lymphocytes, WBC, HGB, granulocytes, HCT, PLT, RBC, MPV, MCV, monocytes, and MCH (Fig. 2F). Furthermore, serum biochemical markers including TBIL, AST, CREA, UA, CK, ALP, BUN, ALT, and LDH were monitored (Fig. 2G) and no statistically significant differences were observed among groups.

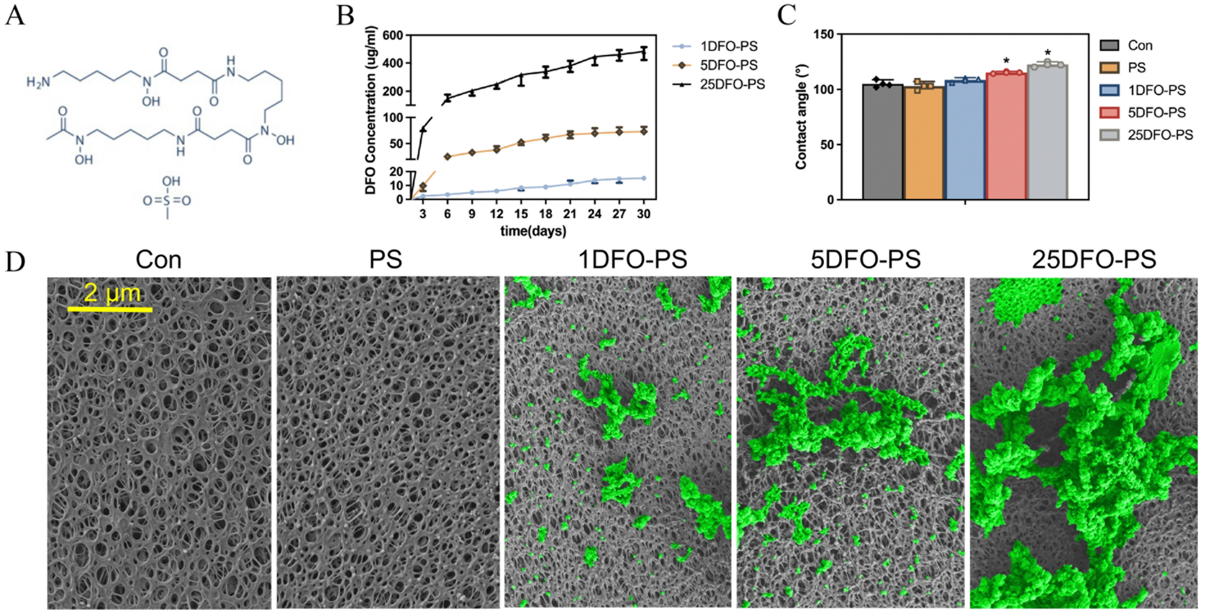

Fig. 1 Material characterization of DFO-PS. (A) Molecular formula of DFO. (B) Drug release curves. (C) Surface liquid contact angles. (D) Scanning electron microscopy (SEM) images with the pseudocolored green regions indicating the loaded DFO.

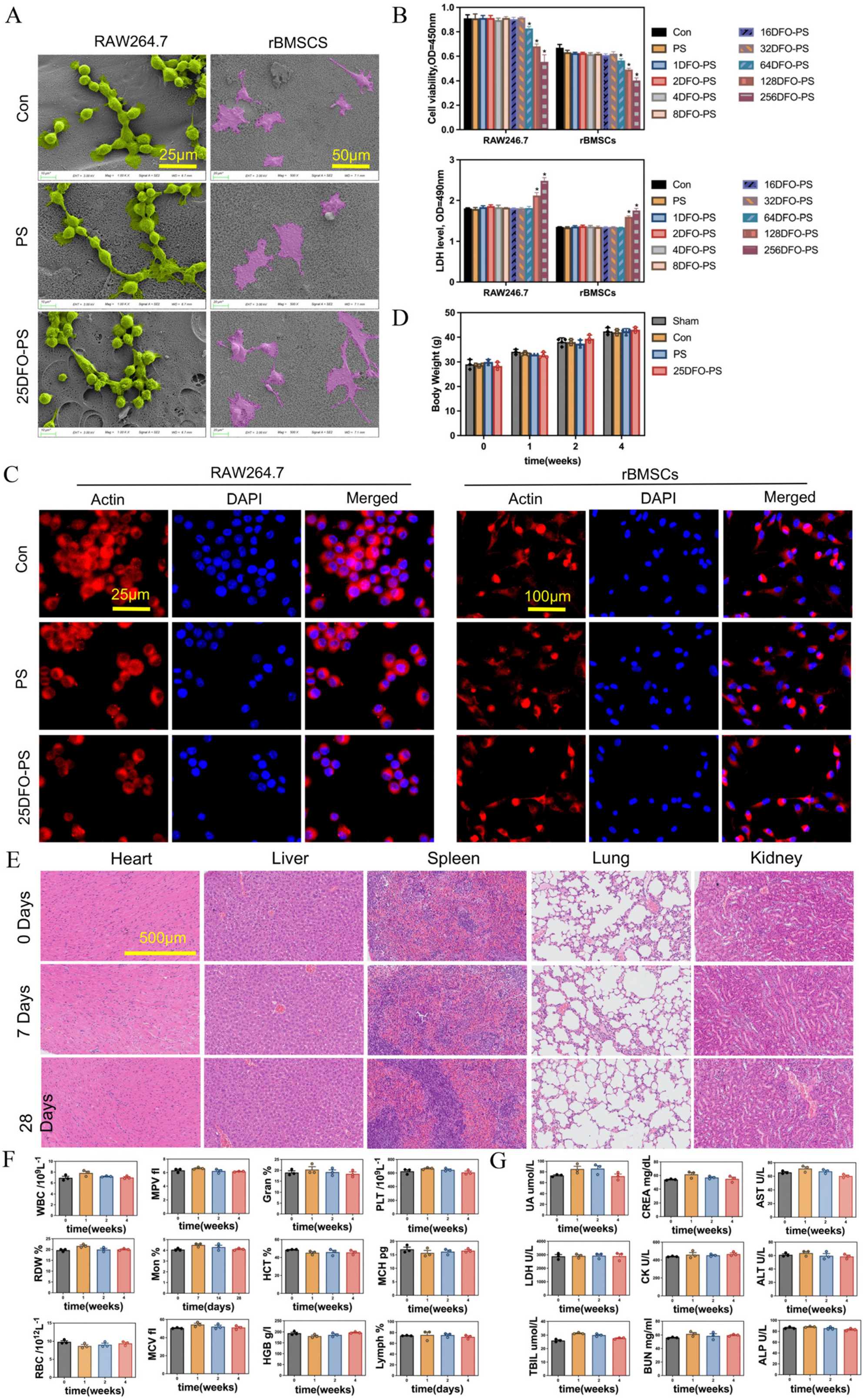

Fig. 2 Biocompatibility analysis of DFO-PS *in vitro* and *in vivo*. (A) Representative scanning electron microscopy (SEM) micrographs of RAW264.7 macrophages and rat bone marrow mesenchymal stem cells (rBMSCs). (B) Cell viability using the CCK8 assay and LDH release levels in RAW264.7 cells and rBMSCs following co-cultivation with DFO-PS for 3 days. (C) Immunofluorescence staining highlighting actin in RAW264.7 cells and rBMSCs following co-cultivation with Con, PS or 25DFO-PS, respectively, for 3 days. (D) Changes in body weights. (E) Histological examination of major organs using HE staining. (F) Dynamic changes in peripheral blood cell counts. (G) Dynamic changes in peripheral blood biochemical markers.

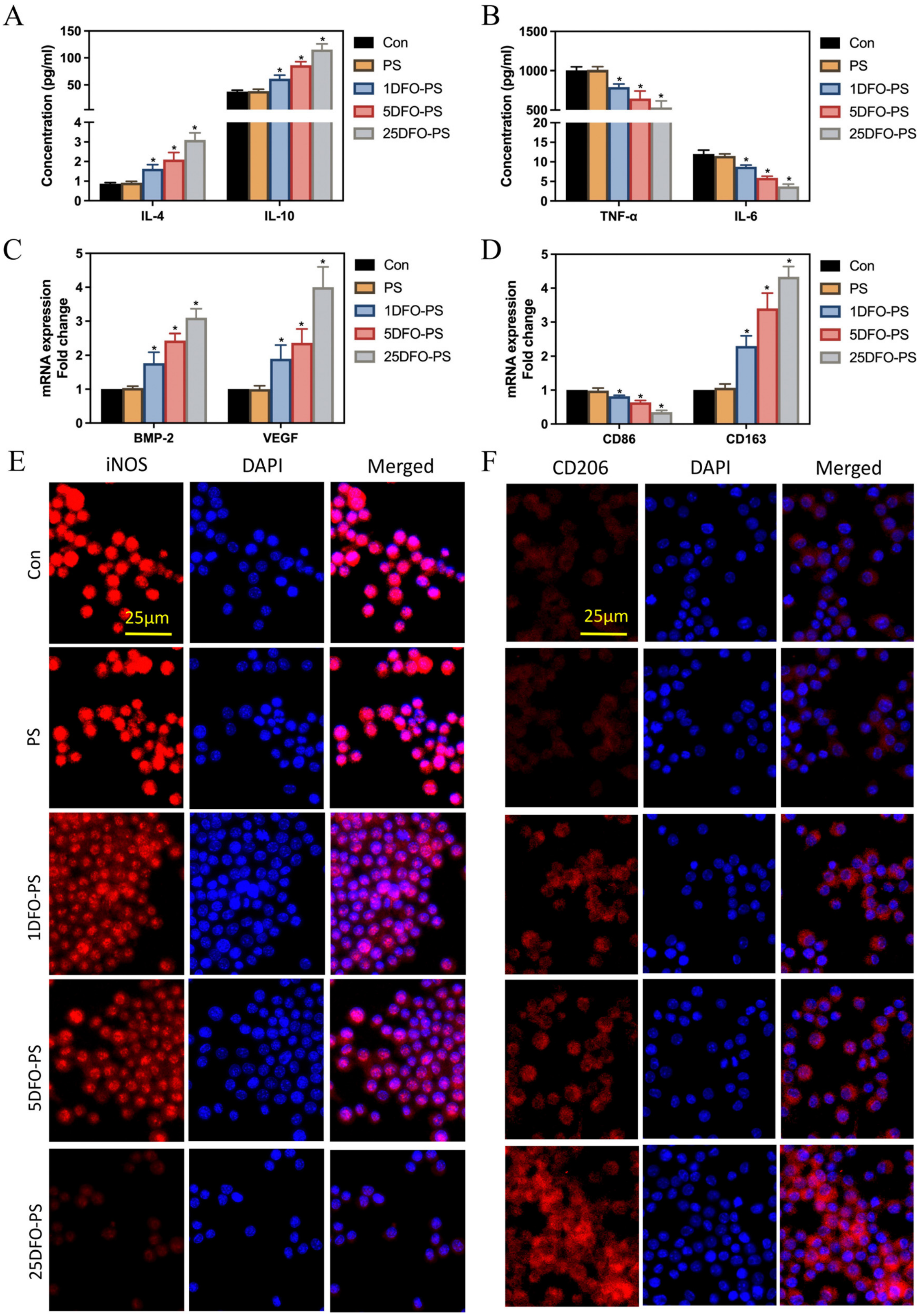

Fig. 3 Modulation of DFO-PS on macrophage polarization *in vitro*. Following 3-day co-culture of RAW264.7 macrophages with different materials: ELISA quantification of (A) anti-inflammatory cytokines (IL-4 and IL-10) and (B) pro-inflammatory cytokines (TNF-α and IL-6) in cell culture supernatants. (C) Relative mRNA expression levels of tissue repair factors (BMP-2 and VEGF) in RAW264.7 macrophages across different treatment groups. (D) mRNA expression levels of the M1 polarization marker (CD86) and M2 polarization marker (CD163) among different experimental groups. Immunofluorescence analysis of (E) M1 polarization marker (iNOS) and (F) M2 polarization marker (CD206) expression in RAW264.7 macrophages.

These comprehensive analyses demonstrate that, while high concentrations of DFO-PS exhibited cytotoxicity toward RAW264.7 and rBMSCs, the optimized concentration of 25 mg mL^{-1} DFO-PS showed no significant toxicity in both cellular and animal models. Statistical analysis was performed using one-way ANOVA followed by Tukey's *post hoc* test ($p < 0.05$ considered statistically significant).

3.3. Modulation of DFO-PS on macrophage polarization *in vitro*

In vitro studies demonstrated that after 3-day co-culture with RAW264.7 macrophages, DFO-PS significantly enhanced the secretion of anti-inflammatory cytokines, IL-4 and IL-10 (Fig. 3A), while simultaneously suppressing the production of pro-inflammatory cytokines, TNF-α and IL-6 (Fig. 3B). The 25DFO-PS group exhibited the most pronounced anti-inflammatory effects. Additionally, DFO-PS significantly upregulated the expression of osteoinductive factor BMP-2 and tissue repair factor VEGF in macrophages (Fig. 3C).

Further investigations revealed that DFO-PS remarkably induced phenotypic alterations in macrophages. Specifically, DFO-PS treatment resulted in decreased expression of the M1 polarization marker CD86 while increasing the expression of the M2 polarization marker CD163. This phenomenon demonstrated a concentration-dependent manner, where higher DFO loading corresponded to lower CD86 expression and higher CD163 expression levels (Fig. 3D). Immunofluorescence analysis further confirmed that DFO-PS suppressed the expression of the M1 polarization marker iNOS (Fig. 3E) while enhancing the expression of the M2 polarization marker CD206 (Fig. 3F).

These findings demonstrate that DFO-PS effectively promotes M1-to-M2 macrophage polarization *in vitro*, resulting in decreased pro-inflammatory cytokine secretion, enhanced anti-inflammatory cytokine production, and elevated expression of osteoinductive and tissue repair factors.

3.4. Modulation of DFO-PS on macrophage polarization *in vivo*

In vivo studies conducted on peri-implant tissue at 2 weeks post-implantation demonstrated that DFO-PS modulated macrophage polarization in a dose-dependent manner. RT-PCR analysis revealed suppressed expression of M1 marker CD86 mRNA concurrent with enhanced expression of M2 marker CD163 mRNA, exhibiting a clear dose-dependent relationship (Fig. 4A). Analysis of peri-implant tissue demonstrated upregulated expression of osteoinductive factor BMP-2 and tissue repair factor VEGF mRNA levels in DFO-PS treated groups (Fig. 4B).

ELISA analysis of peri-implant tissue revealed that DFO-PS significantly attenuated the secretion of pro-inflammatory

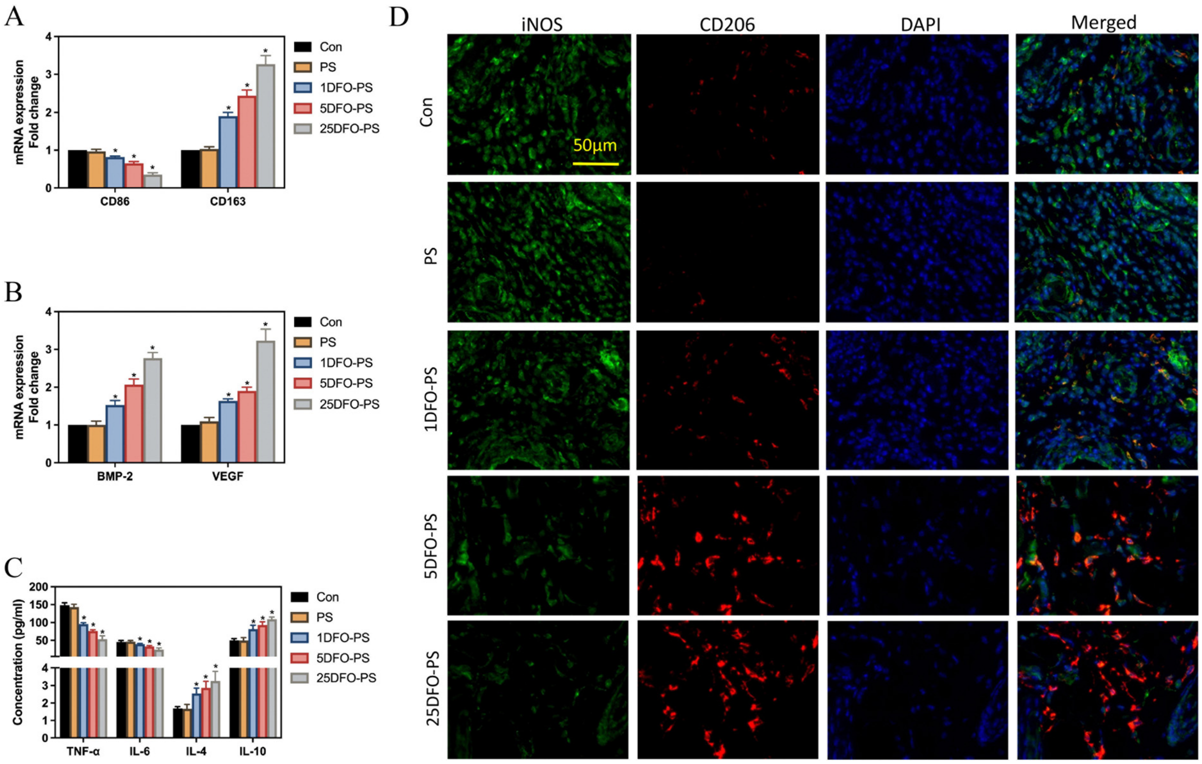

Fig. 4 Modulation of DFO-PS on macrophage polarization *in vivo*. Analysis of peri-implant tissue at 2 weeks post-subcutaneous implantation of DFO-PS in mice: (A) RT-PCR analysis of M1 polarization marker (CD86) and M2 polarization marker (CD163) mRNA expression levels. (B) Quantitative assessment of tissue repair factor (BMP-2 and VEGF) mRNA expression. (C) ELISA quantification of pro-inflammatory cytokines (TNF-α and IL-6) and anti-inflammatory cytokines (IL-4 and IL-10). (D) Immunofluorescence evaluation of M1 polarization marker (iNOS) and M2 polarization marker (CD206) expression.

cytokines TNF-α and IL-6 while enhancing the production of anti-inflammatory cytokines IL-4 and IL-10 (Fig. 4C). The 25DFO-PS group exhibited the most pronounced effects among all treatment groups. Immunofluorescence analysis demonstrated markedly decreased expression of M1 marker iNOS accompanied by significantly enhanced expression of M2 marker CD206. These alterations showed a positive correlation with DFO concentration, where higher DFO loading resulted in more pronounced phenotypic changes (Fig. 4D).

These findings collectively demonstrate that subcutaneous implantation of DFO-PS effectively promotes M1-to-M2 macrophage polarization *in vivo*, characterized by reduced pro-inflammatory cytokine secretion, enhanced anti-inflammatory cytokine production, and elevated expression of osteoinductive and tissue repair factors.

3.5. Direct and indirect macrophage-mediated effects of DFO-PS on rBMSC osteogenic differentiation *in vitro*

The *in vitro* studies demonstrated both direct and macrophage-mediated effects of DFO-PS on rBMSC osteogenic differentiation. Direct co-culture with DFO-PS significantly enhanced rBMSC migration capacity (Fig. 5A) and upregulated the expression of osteogenic-related genes, including ALP, OCN, COL-1, BMP-2, OPN, RUNX2, BSP, and OC (Fig. 5B). The osteogenic potential demonstrated a positive correlation with DFO loading concentration, as evidenced by enhanced ALP activity and increased calcium deposition through ARS staining at day 14 (Fig. 5C).

The indirect effects mediated through macrophage-conditioned medium revealed that RAW264.7 cells treated with DFO-PS secreted factors that significantly enhanced rBMSC chemotaxis (Fig. 5D) and promoted the expression of osteogenic markers (ALP, OCN, COL-1, BMP-2, OPN, RUNX2, BSP, and OC) (Fig. 5E). Furthermore, rBMSCs cultured in macrophage-conditioned medium exhibited enhanced ALP activity and increased matrix mineralization, as demonstrated by intensified ALP and ARS staining at day 14 (Fig. 5F).

These findings demonstrate that DFO-PS promotes osteogenic differentiation of rBMSCs through both direct effects, potentially mediated by surface-enriched DFO, and indirect macrophage-mediated effects *via* modulation of macrophage secretory profiles.

3.6. Osteogenic effects of DFO-PS after 8-week femoral implantation

The osseointegration efficacy of DFO-PS was evaluated in a rat femoral defect model over an 8-week period. Micro-CT analysis revealed enhanced peri-implant bone formation in DFO-PS treated groups (Fig. 6A). Quantitative assessment demonstrated increased BMD, BIC, BV/TV, Tb.N, and Tb.Th values, accompanied by decreased Tb.Sp, indicating enhanced bone growth and remodeling in DFO-PS treated specimens (Fig. 6B).

Sequential fluorescence labeling demonstrated a concentration-dependent increase in new bone formation, with the 25DFO-PS group exhibiting the most substantial osteogenic response (Fig. 6C). Van Gieson staining revealed enhanced collagen fiber formation in the peri-implant region (Fig. 6D), indicating improved extracellular matrix organization and bone formation.

Biomechanical testing demonstrated a significant dose-dependent increase in maximum pull-out force with increasing DFO concentration (Fig. 6E), indicating enhanced implant stability and osseointegration. These findings collectively demonstrate that DFO-PS effectively enhances new bone formation *in vivo*, while simultaneously improving implant stability through enhanced bone-implant integration.

4. Discussion

PEEK has emerged as an outstanding biomaterial for orthopedic applications, offering several crucial advantages. Its mechanical properties closely match human cortical bone, which helps reduce stress shielding, while providing excellent wear resistance and long-term stability. PEEK's clinical benefits include radiolucent properties allowing artifact-free medical imaging, outstanding chemical stability, and proven biocompatibility.[18] Additionally, PEEK's ability to be modified through sulfonation (SPEEK) and its suitability for surface functionalization make it ideal for our application where both mechanical performance and surface modification capability are essential.[19] The incorporation of PDA into our material design strategy plays a crucial role in modulating macrophage responses. PDA's unique surface chemistry, characterized by catechol and quinone groups, enables specific interactions with cell membrane proteins and extracellular matrix components.[20] Studies have demonstrated that PDA-modified surfaces exhibit excellent biocompatibility and can regulate immune cell response.[21] PDA surface modification can effectively reduce the immune response to implanted biomaterials. Specifically, PDA coating decreased macrophage adhesion and activation, leading to reduced inflammatory cell infiltration and fibrous capsule formation around the implants. These findings suggest that PDA surface modification can serve as a simple yet effective strategy to modulate immune responses and improve the biological performance of implanted materials.[22] In this study, DFO-PS was synthesized by combining PDA with SPEEK and loading DFO, utilizing the adhesive properties of the intermediate layer to facilitate functional bone remodeling material formation while employing exogenous stimulation of PDA and DFO to modulate immune responses and promote osseointegration. The findings demonstrate that DFO-PS enhances new bone formation and prosthetic integration through multiple pathways and mechanisms. These results contribute significantly to improving artificial joint adaptability, biocompatibility, and surgical success rates, potentially prolonging post-operative joint functionality, thereby providing crucial guidance and innovation for artificial joint technology development and patient rehabilitation.

This study demonstrated that DFO-PS exhibited excellent properties and biocompatibility. Loading DFO onto the porous surface or within SPEEK effectively enhanced the surface bioactivity and drug release characteristics of DFO-PS. Superior biocompatibility is fundamental for developing next-generation artificial joint prosthesis materials. DFO-PS prepared at concentrations ≤25 mg mL^{-1} exhibited favorable cellular biocompatibility with both RAW264.7 and rBMSCs. Furthermore, weight monitoring, major organ H&E staining,

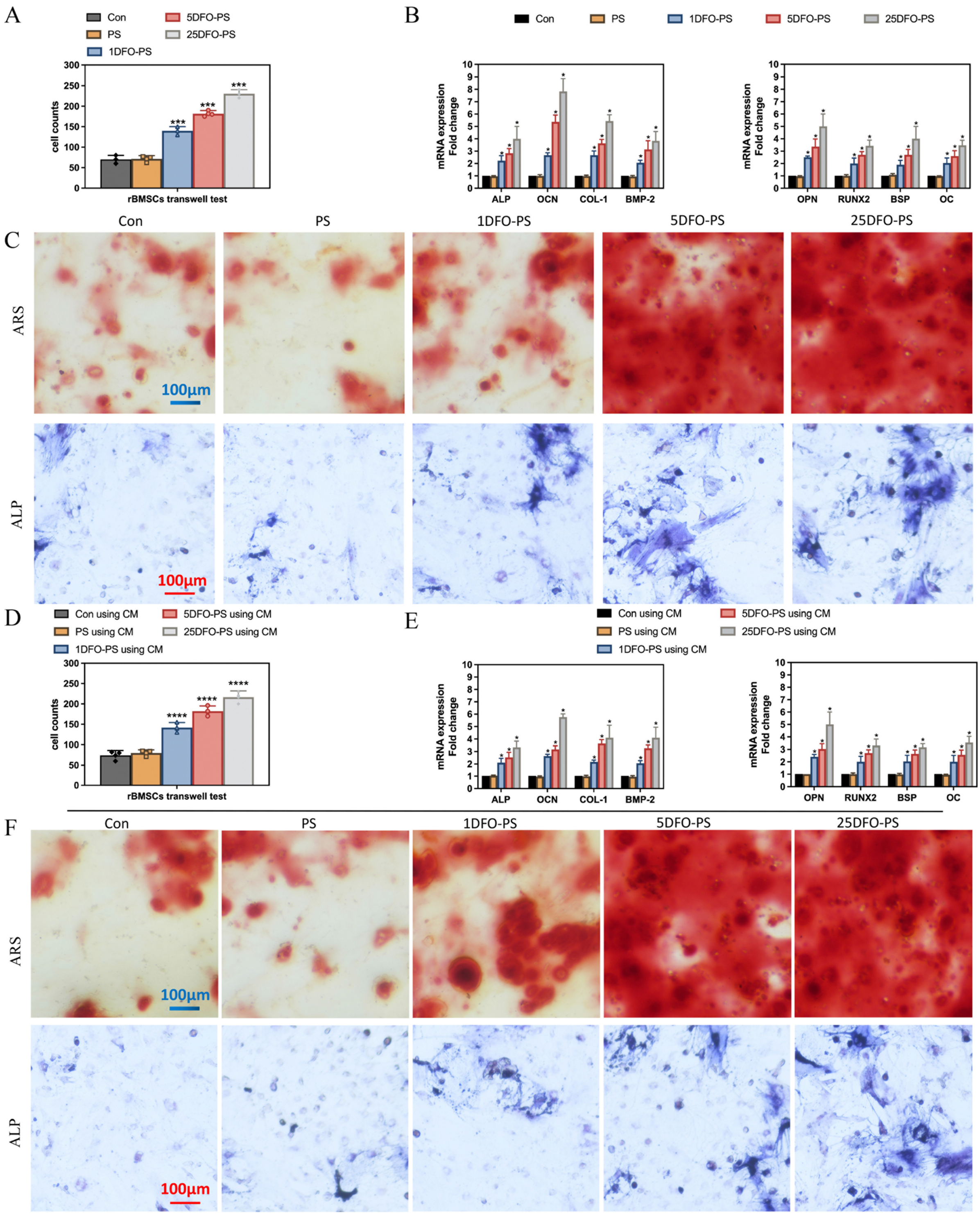

Fig. 5 Direct and indirect macrophage-mediated effects of DFO-PS on rBMSC osteogenic differentiation *in vitro*. Direct effects following 14-day co-culture of DFO-PS with rBMSCs: (A) Transwell migration assay of rBMSCs. (B) Expression analysis of osteogenic-related genes. (C) ALP activity and Alizarin Red S (ARS) staining for extracellular calcium deposition. Macrophage-mediated effects through the macrophage-conditioned medium: Following the 2-day co-culture of DFO-PS with RAW264.7 macrophages, the conditioned medium was collected and applied to rBMSCs for 14 days, analyzing (D) rBMSC migration capacity *via* the transwell assay, (E) oteogenic gene expression profiles, and (F) ALP activity and extracellular matrix mineralization *via* ARS staining.

and peripheral blood cell and biochemical parameter analyses confirmed the excellent *in vivo* biocompatibility of DFO-PS.

Investigation of the synergistic mechanisms between DFO-PS and rBMSCs revealed both direct and indirect osteogenic effects. DFO-PS directly stimulated peri-implant bone growth in

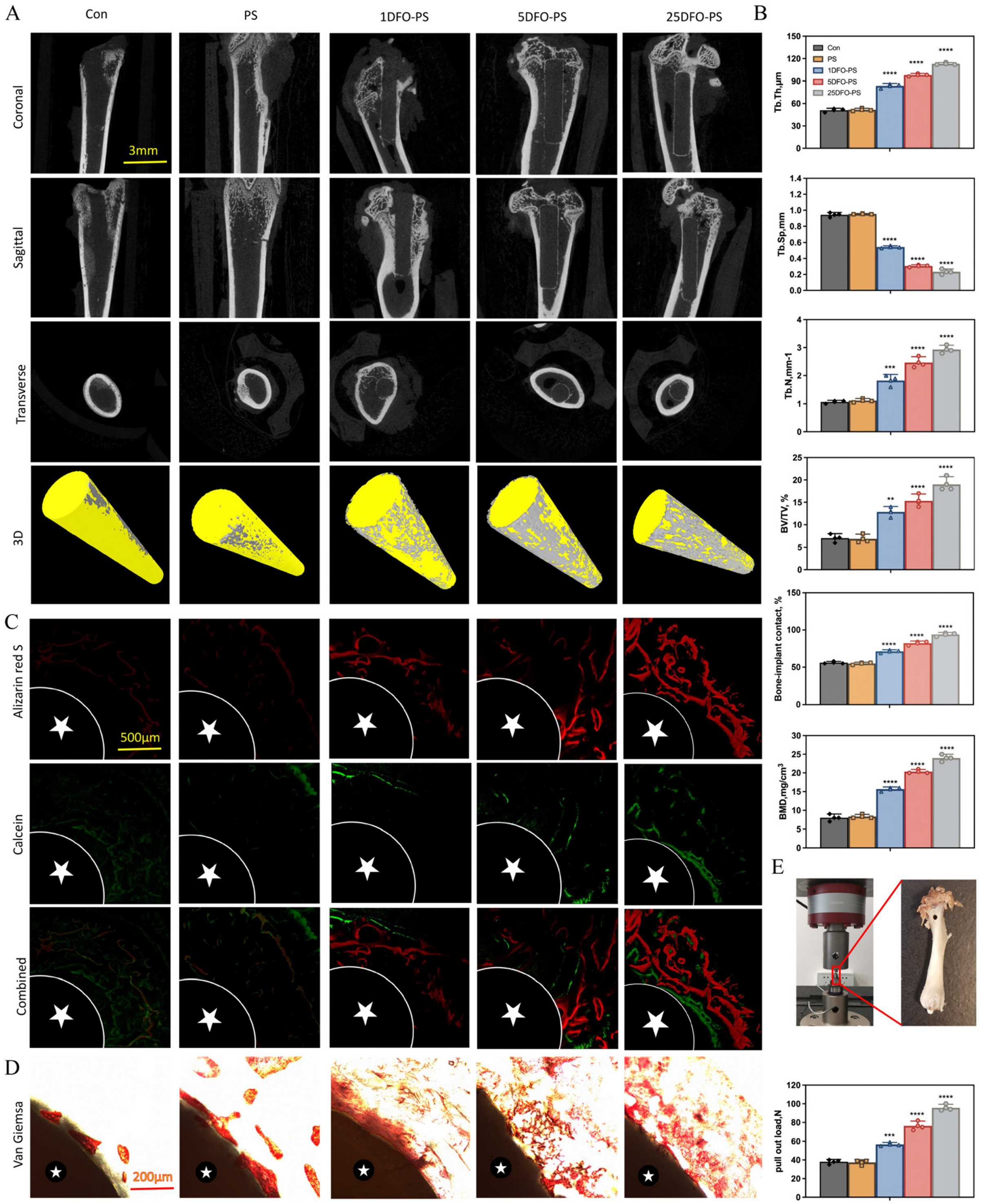

Fig. 6 Osteogenic effects of DFO-PS after 8-week femoral implantation. (A) Micro-CT analysis and 3 dimensional reconstruction of new bone formation. (B) Quantitative bone parameters: Bone mineral density (BMD), bone-implant contact ratio (BIC%), bone volume fraction (BV/TV), trabecular number (Tb.N), trabecular thickness (Tb.Th), and trabecular separation (Tb.Sp). (C) Sequential fluorescence labeling of new bone formation. (D) Van Gieson staining for bone tissues (☆ stands for the implant position of different materials). (G) Pull-out mechanical testing: Schematic experimental procedure and the maximum pull-out force measurements ($n = 3$, $*p < 0.05$, *vs.* control group for B and E; $n = 3$).

rat femur by upregulating target genes involved in rBMSC osteogenic differentiation, including *ALP*, *OCN*, *COL-1*, *BMP-2*, *OPN*, *RUNX2*, *BSP*, and *OC*. These genes encode matrix proteins and transcription factors crucial for osteoblast proliferation, differentiation, and matrix formation. Dey *et al.*[23] demonstrated that Symphytum officinale promotes BMSC osteogenic differentiation genes *RUNX2*, *OPN*, *OC*, and *ALP*, suggesting its potential use in orthopedic implant surface coatings. Ding *et al.*[24] found that ginsenoside compound K induces rBMSC osteogenic differentiation genes and increases new bone BMD, BV/TV, and callus volume. Akshaya *et al.*[25] identified valproic acid as a promising surface modification coating for artificial joint prostheses, showing good affinity with mouse BMSCs and promoting osteogenic differentiation. In this study, it was found that DFO-PS could promote osteogenesis through indirect mechanisms by interacting with RAW264.7 macrophages, releasing osteoinductive factor BMP-2 and tissue repair factor VEGF, which promoted peri-implant bone formation by inducing adjacent mesenchymal stem cell differentiation.

DFO-PS demonstrated significant modulatory effects on macrophage polarization by suppressing M1 markers (CD86 and iNOS) while enhancing M2 markers (CD163 and CD206), thereby facilitating the M1-to-M2 polarization of RAW264.7 macrophages. M1 macrophages are primarily involved in inflammatory responses and early tissue repair, whereas M2 macrophages exhibit anti-inflammatory and tissue-regenerative properties. The M2 macrophage-induced microenvironment has been shown to promote BMSC osteogenic differentiation.[26–28] Recent studies have demonstrated various approaches to enhance osteogenesis through macrophage modulation. Wang *et al.*[29] identified adrenomedullin 2 as an effective joint prosthesis coating that induces M2 polarization and subsequent BMSC osteogenic differentiation, showing favourable bone healing properties in type 1 diabetic rat tibial fracture models. Hamlet *et al.*[30] demonstrated that titanium alloy surface modification significantly upregulated CD163 expression, promoting M2 polarization and enhancing TGF-BMP signaling pathway-related gene expression. β-Tricalcium phosphate (β-TCP), as reported by Zheng,[31] promoted M2 polarization through CD206 upregulation, subsequently enhancing the expression of osteogenic genes including *ALP*, *OPN*, *OC*, *Runx2*, *COL-1*, and *ATF* in BMSCs. Additionally, Romero-Lopez *et al.*[32] found that IL-4-supplemented photocrosslinked methacrylated gelatin 3D hydrogel scaffolds increased CD206, CCL17, and CCL18 expression, creating an osteogenic microenvironment through M2 polarization.

DFO-PS enhanced new bone formation and osseointegration by promoting calcium deposition and collagen fiber formation, thereby strengthening the bone–implant interface. This effect was achieved through reduced pro-inflammatory cytokine secretion (TNF-α and IL-6) and increased anti-inflammatory

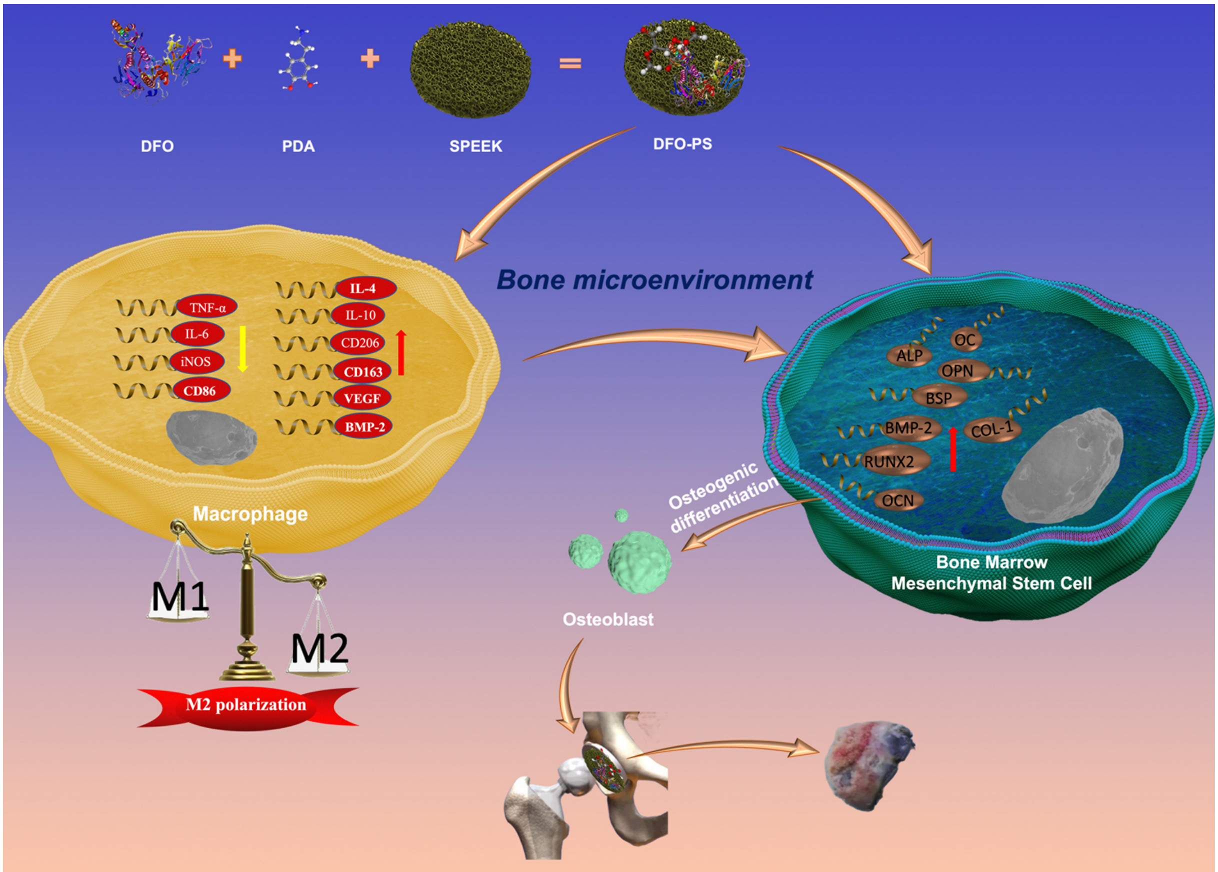

Fig. 7 Mechanisms of DFO-PS-mediated osteogenic differentiation.

factors (IL-4 and IL-10), while simultaneously stimulating osteoinductive factor BMP-2 and tissue repair factor VEGF production. Geng *et al.*[33] demonstrated strontium ranelate's ability to suppress TNF-α and IL-1β secretion while promoting RunX2, OCN, and OPG expression. Kamboj *et al.*[34] developed a 400-μm pore size scaffold using silicon powder and wollastonite, which enhanced IL-8 and TGF-β expression, creating an osteoimmune environment conducive to BMSC differentiation. Croes *et al.*[35] identified TLR-2 activators derived from inactivated *S. aureus* as potential joint interface coatings, demonstrating reduced inflammatory infiltration and enhanced bone formation.

While our current study demonstrates encouraging functional outcomes, including enhanced M2 macrophage polarization, improved angiogenesis, and superior osseointegration by DFO-PS implantation, further mechanistic investigations would strengthen our findings. Building on other researchers' groundbreaking works,[36] our future work will focus on (1) exploring detailed molecular mechanisms, particularly the HIF-1α pathway and its downstream effects; (2) investigating the cross-talk between immune cells and BMSCs in response to DFO-PS; (3) incorporating advanced characterization techniques for surface–biological interactions; (4) examining the temporal relationship between immunomodulation and enhanced bone formation.

In summary, DFO-PS promotes bone regeneration and prosthetic integration through multiple mechanisms as shown in Fig. 7: (1) enhancing osteogenic gene expression (ALP, OCN, COL-1, BMP-2, OPN, RUNX2, BSP, and OC), (2) modulating macrophage polarization from M1 to M2 phenotype, and (3) creating a pro-regenerative microenvironment through cytokine modulation. These findings suggest DFO-PS as a promising component for next-generation joint prostheses with significant clinical translation potential.

5. Conclusions

This study successfully developed DFO-PS, a novel multifunctional material, for artificial joint prostheses, by immobilizing DFO on SPEEK through PDA-mediated modification. DFO-PS demonstrated enhanced osseointegration through multiple mechanisms, including upregulation of osteogenic genes, M1-to-M2 macrophage polarization, and optimization of the local microenvironment. *In vivo* evaluation revealed a 1.22-fold increase in trabecular thickness and a 1.51-fold enhancement in maximum pull-out force compared to controls. These findings establish DFO-PS as a promising candidate for next-generation artificial joint prostheses with integrated biomineralization and immunomodulation properties, offering significant potential for clinical translation.

Data availability

The data supporting this article have been included as part of the ESI.†

Conflicts of interest

All authors declare that they have no competing financial interests or personal relationships that could appear to influence the work reported in this paper.

Acknowledgements

We acknowledge financial support from the National Natural Science Foundation of China (grant no. 82102539 and 82272513) and the Shanghai Sailing Program (grant no. 20YF1436100 and 21YF1433800).

References

1 U. G. Longo, R. Papalia, G. Salvatore, S. M. Tecce, A. Jedrzejczak, M. Marcozzi, I. Piergentili and V. Denaro, *BMC Surg.*, 2022, **22**, 355.
2 D. N. Bracey, K. Barry, H. S. Khanuja and V. Hegde, *J. Am. Acad. Orthop. Surg.*, 2022, **30**, 443–447.
3 H. M. Kremers, J. L. Howard, Y. Loechler, C. D. Schleck, W. S. Harmsen, D. J. Berry, M. E. Cabanela, A. D. Hanssen, M. W. Pagnano, R. T. Trousdale and D. G. Lewallen, *J. Bone Jt. Surg., Am. Vol.*, 2012, **94**, e82.
4 P. Soares Machado, A. C. Cadore Rodrigues, E. T. Chaves, A. H. Susin, L. F. Valandro, G. K. R. Pereira and M. P. Rippe, *J. Adhes. Dent.*, 2022, **24**, 233–245.
5 B. Pidhatika, V. T. Widyaya, P. C. Nalam, Y. A. Swasono and R. Ardhani, *Polymers*, 2022, 14.
6 M. Paglia, M. Beretta, V. Quinzi and S. Colombo, *Eur. J. Paediatr. Dent.*, 2022, **23**, 137–139.
7 N. Muthiah, Y. U. Yolcu, N. Alan, N. Agarwal, D. K. Hamilton and A. Ozpinar, *Eur. Spine J.*, 2022, **31**, 2547–2556.
8 M. L. Alfieri, T. Weil, D. Y. W. Ng and V. Ball, *Adv. Colloid Interface Sci.*, 2022, **305**, 102689.
9 S. El Yakhlifi and V. Ball, *Colloids Surf., B*, 2020, **186**, 110719.
10 E. Schwendich, L. Salinas Tejedor, G. Schmitz, M. Rickert, J. Steinmeyer, S. Rehart, S. Tsiami, J. Braun, X. Baraliakos, J. Reinders, E. Neumann, U. Muller-Ladner and S. Capellino, *Cells*, 2022, **11**, 1609.
11 J. Velasquez and A. A. Wray, *StatPearls*, StatPearls Publishing, Copyright © 2023, Treasure Island (FL), 2023.
12 R. Tevlin, M. T. Longaker and D. C. Wan, *Adv. Wound Care*, 2022, **11**, 548–559.
13 A. Momeni, S. Rapp, A. Donneys, S. R. Buchman and D. C. Wan, *J. Craniofac. Surg.*, 2016, **27**, 880–882.
14 H. Lintel, D. B. Abbas, C. V. Lavin, M. Griffin, J. L. Guo, N. Guardino, A. Churukian, G. C. Gurtner, A. Momeni, M. T. Longaker and D. C. Wan, *J. Transl. Med.*, 2022, **20**, 274.
15 M. Pfeiffenberger, A. Damerau, I. Ponomarev, C. H. Bucher, Y. L. Chen, D. Barnewitz, C. Thone-Reineke, P. Hoff, F. Buttgereit, T. Gaber and A. Lang, *J. Bone Miner. Res.*, 2021, **36**, 1189–1201.
16 W. Liu, J. H. Li, M. Q. Cheng, Q. J. Wang, K. W. K. Yeung, P. K. Chu and X. L. Zhang, *Adv. Sci.*, 2018, **5**, 1800749.

17 S. Sang, C. Yang, H. Chai, X. Yuan, W. Liu and X. Zhang, *Chem. Eng. J.*, 2021, **420**, 130059.

18 P. Sikder, *Acta Biomater.*, 2025, **191**, 29–52.

19 M. Kauke-Navarro, L. Knoedler, S. Knoedler, C. Deniz and A. F. Safi, *Front. Surg.*, 2024, **11**, 1351749.

20 Y. L. Liu, K. L. Ai and L. H. Lu, *Chem. Rev.*, 2014, **114**, 5057–5115.

21 N. Wang, Y. Yang, X. Y. Wang, X. H. Tian, W. X. Qin, X. J. Wang, J. S. Liang, H. J. Zhang and X. F. Leng, *ACS Biomater. Sci. Eng.*, 2019, **5**, 2330–2342.

22 S. K. Hong, K. Y. Kim, H. J. Wook, S. Y. Park, K. D. Lee, D. Y. Lee and H. S. Lee, *Nanomedicine*, 2011, **6**, 793–801.

23 D. Dey, P. Jingar, S. Agrawal, V. Shrivastava, A. Bhattacharya, J. Manhas, B. Garg, M. T. Ansari, A. R. Mridha, V. Sreenivas, A. Khurana and S. Sen, *J. Ethnopharmacol.*, 2020, **248**, 112329.

24 L. Ding, S. Gu, B. Zhou, M. Wang, Y. Zhang, S. Wu, H. Zou, G. Zhao, Z. Gao and L. Xu, *Front. Pharmacol.*, 2022, **13**, 855393.

25 N. Akshaya, P. Prasith, B. Abinaya, B. Ashwin, S. V. Chandran and N. Selvamurugan, *Curr. Mol. Pharmacol.*, 2021, **14**, 27–35.

26 E. Oba, N. Y. Aung, R. Ohe, M. Sadahiro and M. Yamakawa, *Am. J. Transl. Res.*, 2020, **12**, 1728–1740.

27 D. Naot, B. Pool, A. Chhana, R. Gao, J. T. Munro, J. Cornish and N. Dalbeth, *Arthritis Res. Ther.*, 2022, **24**, 212.

28 J. Munoz, N. S. Akhavan, A. P. Mullins and B. H. Arjmandi, *Nutrients*, 2020, **12**, 2999.

29 F. Wang, L. Kong, W. Wang, L. Shi, M. Wang, Y. Chai, J. Xu and Q. Kang, *Stem Cell Res. Ther.*, 2021, **12**, 288.

30 S. M. Hamlet, R. S. B. Lee, H. J. Moon, M. A. Alfarsi and S. Ivanovski, *Clin. Oral. Implants Res.*, 2019, **30**, 1085–1096.

31 M. Zheng, M. Weng, X. Zhang, R. Li, Q. Tong and Z. Chen, *Biomed. Mater.*, 2021, **16**, 025005.

32 M. Romero-Lopez, Z. Li, C. Rhee, M. Maruyama, J. Pajarinen, B. O'Donnell, T. H. Lin, C. W. Lo, J. Hanlon, R. Dubowitz, Z. Yao, B. A. Bunnell, H. Lin, R. S. Tuan and S. B. Goodman, *Tissue Eng., Part A*, 2020, **26**, 1099–1111.

33 T. Geng, X. Chen, M. Zheng, H. Yu, S. Zhang, S. Sun, H. Guo and Q. Jin, *Mol. Med. Rep.*, 2018, **18**, 1849–1857.

34 N. Kamboj, J. Kazantseva, R. Rahmani, M. A. Rodriguez and I. Hussainova, *Mater. Sci. Eng., C*, 2020, **116**, 111223.

35 M. Croes, M. C. Kruyt, W. Boot, B. Pouran, M. V. Braham, S. A. Pakpahan, H. Weinans, H. C. Vogely, A. C. Fluit, W. J. Dhert, J. Alblas and F. C. Oner, *Eur. Cells Mater.*, 2019, **37**, 402–419.

36 X. Shi, Z. W. Liu, X. Y. Ren, W. X. Wang, H. Zhang, Y. G. Wang, M. Liu, Q. Yao and W. G. Wu, *Int. J. Biol. Macromol.*, 2025, **284**, 137968.